Revision 1

Crystal chemical and structural modifications of erionite fibers leached with simulated lung fluids

PAOLO BALLIRANO* AND GEORGIA CAMETTI

Dipartimento di Scienze della Terra, Sapienza Università di Roma - Piazzale A. Moro 5 I-00185 Roma, Italy.

* Corresponding author: Tel. +39 06 49914967

E-mail address: paolo.ballirano@uniroma1.it

ABSTRACT

Inhalation of erionite has been proven to be the cause of the extended epidemic of malignant mesothelioma occurring in Central Anatolia, Turkey and of cases of lung diseases in the USA. Its carcinogenicity is three orders of magnitude greater than that of regulated asbestos. Here we report the results of the investigation of the structural and crystal chemical modifications occurring in erionite leached with artificial lysosomal fluid (ALF) and Gamble's solution. ALF leaching produces a migration of Na^+ ions from Ca1 to Ca2 extraframework cationic site, without the occurrence of any significant modification of the chemical composition of the fibers. Differently, leaching with Gamble's solution induces a complex ionic-exchange process resulting in a temporary partial replacement of Na^+ by Ca^{2+}, coming from the fluid, which is fixed at a third Ca3 cationic site. Subsequently, the exchange process reverses. In fact, Ca^{2+} is removed from Ca3 and Na^+ migrates back to Ca1, the structure being indistinguishable from the starting, unleached material. Such process seems to be accompanied by a progressive amorphization of fibers. Present data are

expected provide a valuable background for a more detailed comprehension of the morphostructural/biological activity relationships inducing pathogenicity.

Keywords: Erionite-Na, malignant mesothelioma (MM), simulated lung fluids SLFs, leaching, Rietveld method

INTRODUCTION

Erionite is a fibrous zeolite belonging to the so-called ABC-6 family (Gottardi and Galli 1985) usually occurring in volcanic ash altered by weathering processes. It is hexagonal, space group $P6_3/mmc$, topological code [ERI] (Baerlocher et al. 2007). The framework consists of columns of double six-rings (D6R) alternating with cancrinite (ε) cages, and columns of erionite cages. In total, a unit-cell contains two D6R, two ε, and two erionite cages. An average chemical formula $K_2(Na,Ca_{0.5})_8[Al_{10}Si_{26}O_{72}] \bullet 30H_2O$ has been proposed for erionite but, owing to a relevant chemical variability, three different species, erionite-K, erionite-Ca, and erionite-Na are recognized (Coombs et al. 1997).

In the past few years erionite has been the object of several investigations because of its linking with malignant mesothelioma (MM). In fact, *in vivo* studies have unambiguously proved that erionite is 500-800 times more tumorigenic than chrysotile and crocidolite asbestos (Coffin et al. 1992) accordingly being included by the International Agency for Research on Cancer (IARC) in the Group 1 Human-Carcinogen list (IARC 1987; 2011). The high rate of MM occurring in several villages of Central Anatolia, Turkey, has been unequivocally related to erionite fibers inhalation in the late 1970s by Baris and co-workers (Baris et al. 1978; Artvinli and Baris 1979). For a few years this environmental problem has been considered as locally circumscribed, until in 1981 the first North American case of erionite-related lung disease was identified in Utah (Rom et al. 1983) and several others were subsequently reported (Ilgren et al. 2008a,b). Since 2005, the concern with the carcinogenic potential of erionite started to capture the interest of the public opinion in the United States owing to the fact that, since 1980s, gravel pits were excavated in areas within the USA

containing erionite (Sheppard 1996), as North Dakota, and the gravel used as building materials. Epidemiological studies revealed a correlation between occupational exposures to erionite fibers and lung diseases (US EPA and NDDH 2010; Ryan et al. 2011). Biological activity of erionite samples from different localities has been demonstrated to be similar (Carbone et al. 2011). Human mesothelial (HM) cells exposed to erionite release high-mobility group box 1 (HMGB1) and secrete tumor necrosis factor-α (TNF-α), similarly to asbestos (Yang et al. 2006; Yang et al. 2010). Besides, its toxicity has been partly ascribed to the effect of ion-exchanged iron, imbibed after inhalation, arising from protein injury (Carr and Frei 1999). Therefore, iron may participate to Fenton chemistry eventually generating reactive oxygen species (ROS) possibly inducing DNA damage (Hardy and Aust 1995; Eborn and Aust 1995). The chemical analyses of several erionite samples revealed the presence of iron, although this zeolite is a nominally Fe-free phase (Eberly 1964; Dogan et al. 2006). However, it has been shown that iron was located at the zeolite surface as iron oxide nanoparticles (Ballirano et al. 2009) or as thin coating of iron-bearing silicates (Cametti et al. 2013). Five mechanistic hypotheses for asbestos carcinogenicity have been proposed (Kane et al. 1996): a) generation of free radicals damaging DNA; b) physical interference with mitosis; c) stimulation of proliferation of target cells; d) provocation of chronic inflammatory reaction producing prolonged release of ROS, cytokines, and growth factors; e) action as co-carcinogens or carriers of chemical carcinogens to the target tissue. Besides, erionite has very peculiar features that are not shared with the six regulated asbestos, five amphiboles and chrysotile (Fubini and Fenoglio 2007) i.e. the very high (external and internal) surface area (Johnson et al. 1992) and the ionic-exchanger behavior. A significant reduction of surface area has been observed as a result of ionic exchange involving K^+ ions (Eberly 1964).

Here we report the results of a multi-analytical crystal-chemical characterization of erionite-Na fibers from Rome, Oregon (USA) before and after leaching into artificial lysosomal fluid (Moss 1979) (ALF) and Gamble's solution (Marques 2011). ALF is analogous to the fluid with which inhaled particles would come into contact after phagocytosis by alveolar and interstitial

77 macrophages. Gamble's solution simulates the interstitial fluid deep within the lung. Leaching of
78 asbestos fibers into simulated lung fluids (SLFs) has been routinely performed to date for
79 exclusively testing bio-solubility and bio-durability of asbestos (De Meringo 1994). The selection of
80 the two fluids has been performed following the suggestion of NIOSH for solubility assays (Nelson
81 et al. 2009). The investigation aims at exploring the exchange mechanisms and the corresponding
82 structural modifications occurring whenever erionite fibers are kept in contact with SLFs as it is
83 reasonable to hypothesize that bulk effects should play some role in the development of lung
84 diseases. In fact, zeolites are cation exchangers and their ability to deeply interact with SLFs is
85 peculiar and is an entirely different property with respect to the essentially surface-driven activity of
86 asbestos. Therefore, present data provide a sound background for a more detailed comprehension of
87 the morphostructural/biological activity relationships inducing pathogenicity, the final target being
88 the identification of an inactivation route. In fact, one of the limits of investigations performed so
89 far on the subject is the lack of a detailed characterization of the fibers used for testing. This fact
90 renders virtually impossible to correlate compositional/structural changes of the fibers with the
91 modifications occurring at the cellular level.

92 ## EXPERIMENTAL METHODS

93 ### Enrichment procedure

Erionite from Rome, Oregon has been used in the present investigation because it has been reported to occur as nearly pure samples. However, a preliminary X-ray powder diffraction pattern indicated a content of erionite of ca. 85 wt.%, the impurities consisting of quartz, feldspar and clay minerals. Therefore, an enrichment procedure was tailored to increase the erionite content to > 95 wt.%. The raw material was ground in an agate mortar and subsequently placed in about 600 ml of distilled water in an 800 ml plastic beaker. The slurry was disaggregated in an ultrasonic processor operating at 200 W for approximately 10 min. At the end of the process the beaker was removed, covered, and placed onto a vibration-insulated surface, to allow the suspension settling for ca. 60 s. The sedimented fraction consisted of the coarse fraction, mainly feldspar, quartz, and larger

aggregates that were not crushed to component mineral size. Such fraction was removed and the supernatant was let to decant into a second beaker for ca. 1 h, allowing the 20-3 μm size fraction to settle down. In zeolite-rich samples, this will generally be a fairly pure zeolite fraction. The remaining supernatant was decanted in a third beaker and allowed to rest for 20 h to obtain the 3-1 μm size fraction. The small residual fraction was put in a fourth beaker and let to decant for 32 h. In Fig. 1a we report the diffraction patterns, collected with a Bruker AXS D8 Focus equipped with a Si(Li) solid state SolX detector, of the separated fraction at different decanting time. At the end of the first step of the process (I 60s), a relevant fraction of quartz and feldspar was removed. At the end of the third step (III 20h) the sample was almost completely enriched in erionite (ca. 95 wt.%). No additional improvement was achieved at 32 h of sedimentation. However, a careful inspection of the powder pattern pointed out that the enrichment obtained during the second cycle does not further improved any more. As a consequence the last separated fraction obtained at the end of the first cycle (III-20h) and those obtained during the second cycle of separation were merged and used for the investigation. The particle size distribution (μm) of the material used for the present study, measured by dynamic light scattering using a Malvern Zetasizer 2000, has the following relevant parameters D*x*10 = 1.59(2), D*x*50 = 4.78(5), D*x*90 = 149(56). Besides, in order to confirm the assignment of iron to contaminants, we monitored, exploiting the capabilities of the solid-state detector, the FeKα and the FeKβ fluorescence lines as a function of the settling time (Fig. 1b). It is apparent the proportionality existing between the clay minerals content, either admixed or adhering to the fibers surface, and the intensity of the iron fluorescence lines.

Leaching procedure

ALF and Gamble's solution were prepared according to standard formulation (Marques et al. 2011). ALF solution has an acidic pH of 4.5, lower than that of Gamble's solution (7.4), and a much higher organic content. A small aliquot (ca. 10 mg) of the enriched erionite sample was dispersed in closed vials filled with the appropriate SLFs. Nevertheless, it is worth noting that, in principle, present experimental conditions show a relevant difference with respect to those existing *in vivo*. In

fact, SLFs are continuously renewing within the lung, this fact assuring a fairly constant composition of the fluid in contact with the fibers. However, the solid/fluid ratio of those leaching experiments is very small and the overall compositional change of the fluid in contact with the fibers is expected to be irrelevant. The fibers were kept in contact at room temperature (RT) with the solutions for 48 h and 4 months (ALF: ALF-48h, ALF-4m), and for 48 h, 15 d, and 4 months (Gamble's solution: G-48h, G-15d, G-4m), respectively. Each sample was then recovered by filtering, using a nitrocellulose filter membrane with a pore size of 0.22 μm, and dried at RT. Besides, a qualitative chemical analysis of the ALF solution recovered from filtering of the leaching experiment for 48 h, was carried out by Inductive Coupled Plasma Atomic Emission Spectroscopy (ICP-AES), using a Varian Vista RL CCD simultaneous spectrometer.

Scanning electron microscopy (SEM)

The micro-chemical characterization was performed with a FEI Quanta 400 SEM equipped with an EDX Genesis EDS system. Operating conditions were: 15 kV accelerating voltage, 11 mm working distance, 0° tilt angle. Chemical analyses were collected by dispersing a small aliquot of fibers in distilled water in a beaker and subsequently pipetting and depositing a few droplets of the dispersion onto a stub (Cametti et al. 2013). This procedure was carried out to avoid the contribution to the chemical data of impurities still persisting despite the enrichment procedure (Cametti et al. 2013). Final crystal chemical formulae were calculated, after renormalization of the chemical analyses hypothesizing a water content of 18.5 wt.% (corresponding to *ca*. 30 water molecules per formula unit *pfu*), on the basis of 36(Si+Al) atoms per formula unit (*apfu*) (Table 1). Chemical formulae have been calculated from the average of the chemical analyses of each sample passing both the balance error (E%) (Passaglia 1970) and the Mg-content tests (Dogan and Dogan 2008). In addition, two further discriminating factors were imposed. The first one is represented by the potassium content. In fact, potassium should fully occupy the two cancrinite-cages occurring within the erionite structure fixing a lower limit of 2 K *apfu*. Therefore, only those analyses reporting a content of K ≥ 1.9 *apfu* were considered as positive. The total EF cation site scattering

represents the second factor. An analysis of the large data set of reference electron microprobe analyses (EMPA) of prismatic erionite crystals (Passaglia et al. 1998) revealed a total EF cation *s.s.* in the 94-143 e^- range. Those analyses are expected to be reliable as they are relatively immune to the analytical problems occurring during the analysis of fibrous materials by both SEM-EDX and EMPA. As a result, only those analyses exceeding a calculated *s.s.* for EF cations of 90 e^- were considered as positive in the present investigation. It is worth noting that a large fraction of reference chemical analyses of erionite fibers do not pass those extra discriminating factors.

X-ray powder diffraction (XRPD)

The starting material and the leached samples were loaded into 0.5 mm diameter borosilicate capillaries. XRPD data were collected in transmission mode, up to a $(\sin\theta/\lambda)_{max}$ of 0.619 $Å^{-1}$, using a parallel-beam Bruker AXS D8 Advance diffractometer operating in θ-θ geometry, equipped with Göbel mirrors on the incident beam, Soller slits on both incident and (radial) diffracted beams, and a PSD VÅNTEC-1 detector. Such experimental set-up has been proven to produce data of excellent quality almost free from texture (Ballirano 2011a,c). Experimental details of the XRPD data collection are reported in Table 2. Despite of the applied enrichment procedure, a mixed Rietveld/Pawley method was adopted to take into account the small contributions of impurities i.e. phyllosilicates and quartz incompletely removed from the sample. The Pawley method consists of a least square refinement of the diffraction profile in the absence of a structural model, by varying the unit cell parameters and the peak profile parameters. The present diffraction data were fitted by this mixed approach, by inserting a starting structure for erionite and quartz (le Page and Donnay 1976) (ca. 0.2 wt.%), and by applying the Pawley method, adding one additional phase without a reference structural model for clay minerals, approximated by a nontronite-type lattice. The reference nontronite lattice was that reported in Powder Diffraction File 34-0842 i.e. space group *P*3, a = 5.26 Å and c = 14.92 Å (Eggleton 1977). The structural refinement was carried out using TOPAS v.4.2 (Bruker AXS 2009). Peak shape was modeled through FPA (Fundamental Parameters Approach), imposing the following full axial parameters: divergence slit: 0.3°, source length 12 mm, sample

length and receiving slit length 11 mm. The starting structural model consists, a part of the framework atoms, of five extra-framework (EF) cationic sites, K1, K2, Ca1, Ca2, and Ca3; and six water molecules sites (OW7, OW8, OW9, OW10, OW11, and OW12) (Alberti et al. 1997; Cametti et al. 2013). Both the occupancy of all EF cationic and water molecules sites and the isotropic displacement parameters of all sites were refined. However, because of the occurrence of correlations, displacement parameters of the sites were constrained as follow: $B_{T1} = B_{T2}$; $B_{O1} = B_{O2} = B_{O4}$; $B_{O3} = B_{O5} = B_{O6}$; $B_{K1} = B_{K2}$; $B_{Ca1} = B_{Ca2} = B_{Ca3} = B_{Ow8} = B_{Ow9} = B_{Ow10} = B_{Ow11} = B_{Ow12} = 2*B_{Ow7}$. Refinements revealed that only sample G-48h had non-zero electron density at Ca3. Absorption was modeled following the Sabine model for cylindrical samples (Sabine et al. 1998) and the background was fitted by a Chebychev polynomial of the first kind. The occurrence of preferred orientation was tested by means of spherical harmonics (four refinable parameters up to the 6^{th} order). The choice of the number of terms to be used has been performed following the procedure described by Ballirano (2003). As expected for capillary mounts, only marginal improvement of the fit were observed as a result of the nearly absence of texture. Careful scrutiny of diffraction patterns of G-15d and G-4m samples indicates the occurrence of a broad hump located at the high-angle side of the strong 100 reflection of erionite. This hump has been related to a progressive amorphization of erionite and has been fitted including a peak phase at a 2θ position of ca. 8.3° and a crystallite size of 5.7 nm. Final Rietveld plots are shown in Fig. 2, miscellaneous data of the refinements in Table 2. Full structural data of erionite of the various samples have been deposited under the form of CIF files.

RESULTS AND DISCUSSION

Morphological and microchemical characterization

Fibers, generally shorter than 30 μm and having a diameter ranging from ca. 0.5 to ca. 2.5 μm, are actually composed of fibrils with individual diameters of ca. 0.1 μm (Fig. 3). The permanence of the fibers in contact with SLFs does not alter their morphology suggesting that only a minor, regular

176 digestion occurs in the case of the leaching with the acidic ALF solution, at least within the period
177 of time investigated. In fact, qualitative ICP-AES analyses of the filtered leaching fluid indicate that
178 Si and Al have been partly solubilized.

179 According to the chemical data the investigated sample has been classified as erionite-Na.
180 Microanalyses rule out the presence of iron and calcium into both untreated erionite fibers and those
181 leached with ALF. On the contrary, in the case of G-48h a significant amount of Ca^{2+} has been
182 detected by SEM-EDX analysis. As will be shown below, the structural refinement disclosed the
183 attribution of Ca^{2+} as EF cation located within the erionite cage. The calculated R = Si/(Al+Si) ratio
184 of 0.794(11) is smaller than 0.807 reported for erionite-K from the same locality (Ballirano et al.
185 2009). The potassium content exceeds 2 K *apfu*. As far as the exchange mechanism is referred to,
186 the chemical data reveal that after leaching with the ALF solution the composition suffers only very
187 marginal modifications with respect to the starting material. On the contrary, leaching with
188 Gamble's solution induces in G-48h an ionic-exchange process consisting in a partial replacement
189 of Na^{+} by Ca^{2+}, originally absent into the untreated fibers, which is progressively (G-15d and G-
190 4m) replaced back by Na^{+}. Besides, a very limited increase of the potassium content has been
191 observed in G-48h, G-15d, and G-4m coherently with the presence of K^{+} ions into Gamble's
192 solution, differently from ALF. This behavior agrees with the reported strong preference of erionite
193 for K^{+} and a good preference of Ca^{2+}, at low levels of divalent cations (Sherry 1979). The R =
194 Si/(Al+Si) ratio does not significantly modify during the leaching process as indicated by an
195 average value of 0.793(4).

196 **Structural modifications**

197 The basic structural features of the erionite framework are known in reasonable detail (Galli and
198 Gottardi 1985; Baerlocher et al. 2007). Extra-framework cations are located as follow: each
199 cancrinite cage hosts a potassium ion (site K1) whereas up to a maximum of three Ca1, Ca2, and
200 Ca3 EF cations sites are situated along the axis of each erionite cage (Fig. 4). Besides, a further K2
201 site, located at the center of the boat-shaped 8-member rings (8MR) forming the walls of the

erionite cage, has been found in erionite-K and assigned to extra potassium ions (Ballirano et al. 2009).

In spite of the different EF cations content of the two samples, cell parameters of the starting material are similar to those of erionite-K from Rome (Ballirano et al. 2009). The effect of leaching is a volume contraction arising from the *a*-parameter shortening partly counterbalanced by a smaller *c*-parameter expansion (Table 3). Prolonged leaching with Gamble's solution, after an initial volume contraction, produces a convergence of the cell parameters toward those of the starting material. In the case of leaching with ALF, the behavior follows a similar trend albeit extremely slowed down. Volume-weighted mean column height L_{vol} and ε_0 micro-strain (lattice strain) were obtained from evaluation of the integral breadths β_i of the individual reflections (Ballirano and Sadun 2009). The refined L_{vol} value (corresponding to the coherency domain) compares favorably with the diameter of a single fibril as observed by SEM. In the case of fibers kept in contact with ALF, L_{vol} irregularly reduces as a function of the leaching time whereas ε_0 is unchanged at the 1σ level. Differently, in the case of leaching with Gamble's solution, both L_{vol} reduction and ε_0 increase follows a regular path.

The mean T-O bond distances of erionite-Na, <T1-O> = 1.630 Å and <T2-O> = 1.652 Å, indicate a partly disordered Si/Al distribution (<T1-O> - <T2-O> = -0.022 Å) consisting in a preferential partition of Al at the T2 site (Table 4). This result agrees with our previous structure refinements of fibrous erionite samples (Ballirano et al. 2009; Cametti et al. 2013). The R ratio, calculated from different methods, based on both evaluation of individual T-O bond distances (Jones 1968; Alberti et al. 1990) and cell volume (Passaglia et al. 1998), takes values in the 0.783-0.804 range, reasonably close to 0.794(11) from chemical data. In particular, the population of the T1 ($Al_{3.99}Si_{20.01}$) and T2 ($Al_{3.83}Si_{8.17}$) sites, consistent with an R-value of 0.783(19), was determined using the Jones' determinative curve (Jones 1968). The value between brackets indicates the estimated standard deviation calculated, from error propagation, taking into account the average standard deviation of the individual T-O bond distances of 0.003 Å (T1-O) and 0.004 Å (T2-O). It

should be pointed out that a difference of <T-O> of 0.001 Å corresponds to a difference of R of ca. 0.004.

The effect of the prolonged contact with both SLFs does not induce significant modification of the R value, whose average is of 0.793(10), incidentally in perfect agreement with 0.793(4) from SEM-EDX data. In the case of the leaching with ALF, a possible marginal de-aluminification process could be expected as a result of the acidic pH of the solution (Piguzova et al. 1965). However, this hypothesis is supported neither by chemical nor by structural data. Besides, T-O-T bond angles show very marginal modifications, generally smaller than 1° (Table 5), indicating the occurrence of extremely limited framework rearrangements.

Chemical data indicate a total site scattering of 96.4 e^- for the EF cations of the untreated material. This value is in reasonable agreement with the *s.s.* of 115(2) e^- obtained from the Rietveld refinement (Table 6). The relatively low *s.s.* from chemical data may be attributed to the effect of alkalis volatilization. Similarly, a total of 32(2) water molecules *pfu* has been obtained from the refinement, in good agreement with reference data (Coombs et al. 1997; Ballirano et al. 2009). The structure of erionite-Na strongly resembles that of erionite-K from the same locality. Differences are restricted to a different EF cations partition between Ca1 and Ca2 sites, and the corresponding different population scheme of the water molecules sites (Table 6). Besides, in the case of erionite-Na both EF cations sites are located at (1/3, 2/3, *z*), along the three-fold axis, instead of being slightly displaced off-axis as in erionite-K. Electron density was detected at the K2 site and, consistently with the chemical analysis, attributed to K exceeding 2 *apfu* (Table 7). Bond valence analysis (Breese and O'Keeffe 1991) confirms that this site can be filled exclusively by K^+ ions. We note that the refined site scattering is in excess with respect to the potassium content quantified by SEM-EDX. According to the large coordination number and the corresponding weak K-O bonds it is possible to hypothesize a K^+ mobilization, from the K2 site, occurring during the micro-chemical analysis. This fact justifies the presence in literature of several chemical analyses pointing out to a K content < 2 *apfu*, which is unsupported by structural requirements (Cametti et al. 2013). Both Ca1

and Ca2 sites have *s.s.* of ca. 30 e^-. Following reference data (Ballirano et al. 2009; Cametti et al. 2013) all available Mg^{2+} was located at Ca1 and the exceeding site scattering was attributed to Na^+. The remaining Na^+ was assigned to Ca2. As it is expected that Na and Mg are occupying very close sites, not resolvable with the present data quality, the corresponding coordination-types are fairly distorted. The occurrence of Mg^{2+} ions at Ca1 and that of K2 site are mutually excluding. In fact, the presence of the OW9 water molecule site, required to provide six-fold coordination to Mg^{2+}, is incompatible with that of K2 owing to a very short K2-OW9 distance of 1.93(4) Å (Fig. 5). An independent confirmation of this restraint was obtained from a check of reference EMPA data (Passaglia et al. 1998), which reveals that potassium contents significantly exceeding 2 K *apfu* consistently correlate with low Mg contents. Furthermore, we deduce that the occurrence of Mg^{2+} at Ca1 and that of the Ca2 site are mutually excluding due to the short OW8-OW9 contact of 2.14(3) Å. In fact, OW8 is fundamental to provide nine-fold coordination for Na^+ at Ca2.

ALF-48h and ALF-4m share similar structural features. The main difference with respect to the untreated material (Fig. 6a) is the relevant reduction of electron density at Ca1 partly counterbalanced by its increase at Ca2. Besides, a corresponding redistribution of the population of the water molecules sites occurs without significant atomic motion. The final EF cations/water molecules distribution pattern is very similar to that of erionite-K (Ballirano et al. 2009). The depletion of the Ca1 site may be interpreted as arising from Na^+ migration toward Ca2 without any detectable overall compositional variation (Fig. 6b, c). ALF-4m has a Ca1 *s.s.* of 5.4(12) e^- corresponding to 0.45(10) Mg *apfu* in excellent agreement with 0.47 Mg *apfu* from chemical data. In effect, the total EF cations *s.s.,* as obtained from the Rietveld refinement, decreases from ca. 115 e^- of the starting material to ca. 92 e^-. However, such reduction is partly counterbalanced by the increase of the total water molecules sites *s.s.* from ca. 260 to ca. 270 e^-. This result is consistent with the partial migration of EF cations toward alternative sites close to the water molecules observed during the thermally induced dehydration of erionite (Ballirano and Cametti 2012).

Instead, G-48h and G-15d show peculiar structural features. In fact, G-48h experiences a reduction of *s.s.* at Ca1, which is counterbalanced by the appearance of electron density at Ca3. The occurrence of this site has been reported in erionite-Ca from Nizhnyaya Tunguska, Siberia (Alberti et al. 1997). Therefore, we propose that this structural modification is induced by the $Ca^{2+} \rightarrow Na^{+}$ ionic-exchange process, which was firstly disclosed from the micro-chemical data (Fig. 6d). In fact, the refined *s.s.* at Ca3 is in reasonable agreement with the Ca *apfu* from SEM-EDX. Nevertheless, bond distances analysis indicates, similarly to erionite-Ca (Alberti et al. 1997), an anomalous coordination of Ca2. In fact, reference data indicate a six-fold coordination to 3 x OW8 at 2.41(3) Å and 3 x O5 at 3.07(2) Å which is incompatible with the available Mg^{2+}, Ca^{2+}, Na^{+}, and K^{+} EF cations (Alberti et al. 1997). However, the corresponding very large anisotropic displacement parameters, both in the *xy* plane and along the *z* direction, could be related to the occurrence of static disorder. We hypothesize that the same reasoning applies for the present refinement.

The occurrence of the three Ca1, Ca2, and Ca3 sites imposes restraints due to short cation-cation contacts. In the case of the exclusive presence of Ca1 and Ca2, no restraints are imposed due to Ca1-Ca1, Ca1-Ca2, and Ca2-Ca2 contacts exceeding 2.9 Å. Therefore, a maximum of 8 non-K EF cations can be in principle hosted by the two erionite cages occurring in the erionite unit-cell. Nevertheless, we have pointed out that the occurrence of Mg^{2+} at Ca1 is incompatible with that of Ca2 site due to short OW8-OW9 contacts. We suppose that this constraint is the reason for Mg contents never exceeding 0.85 *apfu* reported in literature and the corresponding maximum total of non-K EF cations barely exceeding 6 *apfu* reported in reference data for erionite-Na samples (Passaglia et al. 1998). Besides, those samples show potassium contents significantly exceeding 2 *apfu*. The latter feature seems to be typical of erionite-Na.

In the case of the occurrence of all three EF cations sites, Ca3 content is restrained by the maximum site occupancy of 0.5 imposed by Ca3-Ca3 short contacts. Similarly, adjacent Ca1 and Ca2 sites are mutually excluding. Approximately the same EF cations sites filling rules can be devised from analysis of the structural data of erionite-Ca (Alberti et al. 1997). The existence of

305 those restraints is consistent with the observation that erionite-Ca samples generally do not exceed a
306 maximum of 5 non-K EF cations (Alberti et al. 1997; Passaglia et al. 1998). Interestingly, G-15d
307 and G-4m progressively undergo a new exchange process that lead to a refilling of Ca1 and a
308 complete removal of Ca^{2+} from Ca3 (Fig. 6e, f), which is confirmed by SEM-EDX data, and its
309 corresponding replacement by Na^{+}. In particular, Ca^{2+} removal is followed by precipitation of
310 calcite $CaCO_3$, which is clearly evident in Fig. 7, for G-4m. It is worth remarking that this process is
311 subsequent to the full removal of Ca from the erionite structure, which is already completed in G-
312 15d. As a final result, both structure and chemical composition of G-4m are insignificantly different
313 from those of the starting material. The only minor difference is represented by a moderate increase
314 of the potassium content at K2. Besides, Fig. 7 clearly provides evidence of the onset of erionite
315 amorphization as leaching time with Gamble's solution increases. This phenomenon is testified by
316 the growing of a bump located near the high-angle tail of the strong 100 reflection of erionite. We
317 speculate that amorphization proceeds from the outer surface of fibers therefore inducing the
318 reduction of their coherency domain evidenced by the progressively decreasing L_{vol}.
319 Simultaneously, the volumetric expansion of the amorphous shell induces a growing lattice strain
320 consistent with the ε_0 dependence from leaching time observed from XRPD.
321
322 **IMPLICATIONS**
323 According to present results, leaching of erionite-Na fibers with SLFs induces either ionic
324 mobility or complex ionic-exchange processes. As far as leaching with ALF is referred to, the
325 acidic pH produces a partial digestion of fibers whereas the saline charge of the solution does not
326 produce any significant modification of the chemical composition of erionite. Instead, an internal
327 EF cation motion occurs, leading to a progressive Na^{+} migration from Ca1 to Ca2 and to alternative
328 sites close to water molecules. The final result is an almost perfect segregation of Mg^{2+} at Ca1 and
329 of Na^{+} at Ca2. As it is known that fibers can suffer repeated cycles of phagocytosis by alveolar
330 macrophages (AM), this investigation indicates that such fibers are characterized by significant bio-

persistence under those conditions. In the absence of detailed data for erionite, estimated clearance half-times of amosite and crocidolite asbestos have been measured in years to decades, whereas for chrysotile the available data suggest that the vast majority of fibers are cleared within months (Churg and Wright 1994). Besides, the structural modifications are reached under a relatively short time-scale, possibly during the first engulfment, without any significant ionic exchange with ALF. Under such premises, the effect of those fibers, at this stage of their inhalation, may be only the release, from died AMs, of oxidants, cytokines, and growth factors. That release causes a sustained inflammation lasting as long as the fibers resides in the lung (Fubini and Fenoglio 2007). Differently, leaching with Gamble's solution temporarily produces significant structural modification induced by a larger Ca^{2+} content of the SLF as compared to ALF. In this case, release of Na^{+} from Ca1 is counterbalanced by adsorption from Gamble's solution of Ca^{2+}, which is entrapped at Ca3. This phenomenon is confined to a relatively short leaching time (< 2 weeks) and produces a significant ionic exchange between fibers and the interstitial fluid deep within the lung, simulated by the Gamble's solution. However, for a longer leaching time the structure releases back Ca^{2+} ions to the SLF, reacquiring Na^{+} ions. Owing to this final exchange process, fibers return approximately to the starting composition and structure. This process is followed by precipitation of minor calcium carbonate, possibly occurring because of small, unwanted pH deviations from the original value of 7.4 due to long-term CO_2 diffusion. Differently from ALF leaching, a significant amorphization of erionite is evident from XRPD. This fact could possibly affect the number of sites available for fixing iron ions at the surface as well as the biopersistence of the fibers within the human body. A detailed investigation of the surface of the leached fibers by HRTEM, the aim being to confirm and quantify the kinetics of the amorphization process, is planned. Despite it has been reported as the most mobile among the EF cations throughout heating of erionite-K (Ballirano and Cametti 2012), there is no convincing evidence that Mg^{2+} is released by the fibers to SLFs during leaching. Unfortunately such information would be of paramount importance to confirm/rule out the occurrence of the effects on lipid packing, membrane permeability, as well as counteraction of Ca^{2+}

uptake attributed to Mg^{2+} release from amphibole asbestos reported from *in vitro* experiments (Bergamini et al. 2004; Pacella et al. 2012).

As a further result of this investigation, it has been confirmed the absence of Fe for erionite samples from Rome (Ballirano et al. 2009). Such absence is of relevant interest because Fe has been proposed as one of the causes of carcinogenesis *via* Fenton chemistry and production of free radicals (Kane et al. 1996; Fubini and Aréan Otero 1999; Kamp and Weitzman 1999; Robledo and Mossman 1999). Therefore, it is clear that the only role played by erionite could be that of a passive carrier for vehiculating iron within the respiratory system via iron-bearing materials or ion exchange mechanism occurring within the lung (Eborn and Aust 1995; Carr and Frei 1999). The strong tendency of erionite fibers to be coated by nano/microcrystalline iron-bearing materials (Ballirano et al. 2009) may be related, besides macroporosity, to surface charge. Preliminary results of zeta potential measurements indicate that the heteropolar surface of these fibers is negatively charged (ca. -10 mV) whenever immersed in SLFs and therefore cations are attracted and possibly fixed at the surface, especially those, as iron, characterized by high ionic potential. A negatively charged surface is typical of crocidolite (Light and Wei 1977), amphibole asbestos characterized by a relatively low short-term cytotoxicity to macrophages and hemolyticity, as compared to chrysotile. However, it has been reported a strong positive correlation between zeta potential and hemolytic activity and, in particular for crocidolite, a decrease of the zeta potential (becoming more negative) coupled with an increase of the hemolytic activity as a function of time (Light and Wei 1977). As it is expected that EF cation motion and/or cation exchange may significantly influence the magnitude of zeta potential, we are planning to investigate its dependence from time, of the same erionite-Na fibers analyzed in the present work.

Acknowledgments

Thanks are due to Bice Fubini and two anonymous reviewers whose comments greatly help to improve the readability of the paper. The work has received financial support from Sapienza

383 Università di Roma. We thank A. Pacella and J. Fournier for providing fibrous erionite, S. Valente
384 for SLFs preparation, M. Albano for assistance during SEM-EDX analyses, F. Rinaldi and C.
385 Marianecci for preliminary Zeta Potential measurements, and T. Coppola and S. Mignardi for
386 qualitative ICP-AES analysis.

387 **REFERENCES**

388 Alberti, A., Gottardi, G., and Lai, T. (1990) The determination of (Si,Al) distribution in zeolites:
389 in Barthomeuf D. et al. (eds) Guidelines for Mastering the Properties of Molecular Sieves, Vol. 221
390 NATO ASI series, Plenum Press, New York, pp 145-155.

391 Alberti, A., Martucci, A., Galli, E., and Vezzalini, G. (1997). A reexamination of the crystal
392 structure of erionite. Zeolites, 19, 349-352.

393 Artvinli, M., and Baris, Y.I. (1979) Malignant mesothelioma in a small village in the Anatolian
394 region of Turkey: An epidemiologic study, Journal of the National Cancer Institute, 63, 17-22.

395 Baerlocher, Ch., McCusker, L.B., and Olson, D.H. (2007) Atlas of zeolite framework types, 6th
396 revised version. Elsevier, London, pp. 398.

397 Ballirano, P. (2003) Effects of the choice of different ionisation level for scattering curves and
398 correction for small preferred orientation in Rietveld refinement: the $MgAl_2O_4$ test case. Journal of
399 Applied of Crystallography, 36,1056-1061.

400 Ballirano, P. (2011a) Thermal behavior of natrite Na_2CO_3 in the 303-1013 K thermal range.
401 Phase Transitions, 84, 357-374.

402 Ballirano, P. (2011b) Laboratory parallel beam transmission X-ray powder diffraction
403 investigation of the thermal behavior of calcite: comparison with X-ray single-crystal and
404 synchrotron powder diffraction data. Periodico di Mineralogia, 80, 123-134.

405 Ballirano, P. (2011c) Laboratory parallel beam transmission X-ray powder diffraction
406 investigation of the thermal behavior of nitratine $NaNO_3$: spontaneous stress and structure
407 evolution. Physics and Chemistry of Minerals, 38, 531-541.

Ballirano, P., Andreozzi, G.B., Dogan, M., and Dogan, A.U. (2009) Crystal structure and iron topochemistry of erionite-K from Rome, Oregon, U.S.A. American Mineralogist, 94, 1262-1270.

Ballirano, P., and Cametti, G. (2012) Dehydration dynamics and thermal stability of erionite-K: Experimental evidence of the "internal ionic exchange" mechanism. Microporous and Mesoporous Materials, 163, 160-168.

Ballirano, P., and Sadun, C. (2009) Thermal behavior of trehalose dihydrate (T_h) and β-anhydrous trehalose (T_β) by in-situ laboratory parallel-beam X-ray powder diffraction. Structural chemistry, 20, 815-823.

Baris, Y.I., Sahin, A.A., Ozesmi, M., Kerse, I., Ozen, E., Kolacan, B., Altinörs, M., and Göktepeli, A. (1978) An outbreak of pleural mesothelioma and chronic fibrosing pleurisy in the village of Karain/Urgup in Anatolia. Thorax, 33 181-192.

Bergamini, C., Fato, R., Biagini, G., Pugnaloni, A., Giantomassi, F., Foresti, E., Lesci, G.I., and Roveri, N. (2004) Mitochondria changes induced by natural and synthetic asbestos fibers: studies on isolated mitochindria. Cellular and Molecular Biology, 50 (Suppl.), 691-700.

Breese, N.E., and O'Keeffe, M. (1991) Bond-valence parameters for solids. Acta Crystallographica, B47, 192-197.

Bruker AXS (2009) Topas V.4.2: General profile and structure analysis software for powder diffraction data. Bruker AXS, Karlsruhe, Germany.

Cametti, G., Pacella, A., Mura, F., Rossi, M., and Ballirano, P. (2013) New morphological, chemical, and structural data of woolly erionite-Na from Durkee, Oregon, U.S.A. American Mineralogist, 98, 2155-2163.

Carbone, M., Baris, Y.I., Bertino, P., Brass, B., Comertpay, S., Dogan, A.U., Gaudino, G., Jube, S., Kanodia, S., Partridge, C.R., Pass, H.I., Zeyana, S.R., Steele, I., Tuncer, M., Way, S., Yang, H., and Miller, A. (2011) Erionite exposure in North Dakota and Turkish villages with mesothelioma. Proceedings of the National Academy of Sciences, 108, 13618-13623.

Carr, A., and Frei, B. (1999) Does vitamin C act as a pro-oxidant under physiological conditions? The FASEB Journal, 13, 1007-1023.

Churg, A., and Wright, J.L. (1994) Persistence of Natural Mineral Fibers in Human Lungs: An Overview. Environmental Health Perspectives, 102 (Suppl. 5), 229-233.

Coffin, D.L., Cook, P.M., and Creason, J.P. (1992) Relative mesothelioma induction in rats by mineral fibers: comparison with residual pulmonary mineral fiber number and epidemiology. Inhalation Toxicology, 4, 273-300.

Coombs, D.S., Alberti, A., Armbruster, T., Artioli, G., Colella, C., Galli, E., Grice, J.D., Liebau, F., Mandarino, J.A., Minato, H., Nickel, E.H., Passaglia, E., Peacor, D.R., Quartieri, S., Rinaldi, R., Ross, M., Sheppard, R.A., Tillmanns, E., and Vezzalini, G. (1997) Recommended nomenclature for zeolite minerals; report of the Subcommittee on Zeolites of the International Mineralogical Association, Commission on New Minerals and Mineral Names. Canadian Mineralogist, 35, 1571-1606.

De Meringo, A., Morscheidt, C., Thélohan, S., and Tiesler, H. (1994) In vitro assessment of biodurability: Acellular systems. Environmental Health Perspectives, 102, (Suppl. 5), 47-53.

Dogan A.U., Baris Y.I., Dogan M., Emri S., Steele I., Elmishad A.G., and Carbone M. (2006) Genetic predisposition to fiber carcinogenesis causes a mesothelioma epidemic in Turkey. Cancer Research, 66, 5063-5068.

Dogan, A.U., and Dogan, M. (2008) Re-evaluation and re-classification of erionite series minerals. Environmental Geochemistry and Health, 30, 355-366.

Eberly, P.E. (1964) Adsorption properties of naturally occurring erionite and its cationic-exchanged forms. American Mineralogist, 49, 30-40.

Eborn, S.K., and Aust, A.E. (1995) Effect of iron acquisition on induction of DNA singlestrand breaks by erionite, a carcinogenic mineral fiber. Archives of Biochemistry and Biophysics, 316, 507-514.

Eggleton, R.A. (1977) Nontronite: chemistry and X-ray diffraction. Clay Minerals, 12, 181-194.

Farrugia, L.J. (1997) ORTEP-3 for Windows, University of Glasgow, Scotland.

Fubini, B., and Aréan Otero, C. (1999) Chemical aspects of the toxicity of inhaled mineral dusts. Chemical Society Reviews, 28, 373-381.

Fubini, B., and Fenoglio, I. (2007) Toxic Potential of Mineral Dusts. Elements, 3, 407-414.

Gottardi, G., and Galli, E. (1985) Natural zeolites. Springer-Verlag, Heidelberg, pp. xii + 409.

Hardy, J.A., and Aust, A.E. (1995) Iron in Asbestos Chemistry and Carcinogenicity. Chemical Reviews, 95, 97-118.

IARC (1987) IARC Monographs on the evaluation of the carcinogenic risk to humans. Silica and some silicates. Volume 42, 225-239.

IARC (2011) IARC Monographs on the evaluation of the carcinogenic risk to humans. Arsenic, metals, fibres and dusts. Volume 100 C, 311-316.

Ilgren, E.B., Ortega Breña, M., Larragoitia, J.C., Navarrete, G.L., Breña, A.F., Krauss, E., and Fehér, G. (2008a) A reconnaissance study of a potential emerging Mexican mesothelioma epidemic due to fibrous zeolite exposure. Indoor and Built Environment, 17, 496-515.

Ilgren, E.B., Pooley, F.D., Larragoitia, J.C., Talamantes, M., Navarrete, G.L., Krauss, E., and Breña, A.F. (2008b) First Confirmed Erionite Related Mesothelioma in North America. Indoor and Built Environment, 17, 567-568.

Johnson, N. F., Hoover, M. D., Thomassen, D. G., Cheng, Y. S., Dalley, A., and Brooks, A.L. (1992) In vitro activity of silicon carbide whiskers in comparison to other industrial fibers using four cell culture systems. American Journal of Industrial Medicine, 21, 807-823.

Jones, J.B. (1968) Al-O and Si-O tetrahedral distances in aluminosilicate framework structures. Acta Crystallographica, B24, 355-358.

Kamp, D.W., and Weitzman, S.A. (1999) The molecular basis of asbestos induced lung injury. Thorax, 54, 638-652.

Kane, A.B., Boffetta, P., Saracci, R., and Wilbourn, J.D. (1996) Mechanisms of fibre carcinogenesis, 157 p. IARC Scientific Publication 140, Lyon, France.

le Page, Y., and Donnay, G. (1976) Refinement of the Crystal Structure of Low-Quartz. Acta Crystallographica, B32, 2456-2459.

Light, W.G., and Wei, E.T. (1977) Surface charge and asbestos toxicity. Nature, 265 537-539.

Marques, M.R.C., Loebenberg, R., and Almukainzi, M. (2011) Simulated biological fluids with possible application in dissolution testing. Dissolution Technologies, 18, 15-28.

Moss, O.R. (1979) Simulants of lung interstitial fluid. Health Physics, 36, 447□448.

Nelson, A.R., Liverman, C.T., Eide, E.A., and Abt, E. (2009) A Review of the NIOSH roadmap for research on asbestos fibers and other elongate mineral particles. The National Academies Press, Washington DC, Usa, pp. xiv + 120.

Pacella, A., Andreozzi, G.B., Fournier, J., Stievano, L., Giantomassi, F., Lucarini, G., Rippo, M.R., and Pugnaloni, A. (2012) Iron topochemistry and surface reactivity of amphibole asbestos: relations with in vitro toxicity. Analytical and Bioanalytical Chemistry, 402, 871-881.

Passaglia, E. (1970) The crystal chemistry of chabazites. American Mineralogist, 55, 1278-1301.

Passaglia, E., Artioli, G., and Gualtieri, A. (1998) Crystal chemistry of the zeolites erionite and offretite. American Mineralogist, 83, 577-589.

Piguzova, L.I., Nikolina, V.Ya., Dubinin, M.M., and Shishakova, T.N. (1965) Acid resistance of erionite – a synthetic zeolite. Chemistry and Technology of Fuels and Oils, 1, 787-789.

Robledo, R., and Mossman, B. (1999) Cellular and molecular mechanisms of asbestos-induced fibrosis. Journal of Cellular Physiology, 180, 158-166.

Rom, W., Casey, K., Parry, W., Mjaatvedt, C., and Moatamed, F. (1983) Health implications of natural fibrous zeolites in the Intermountain West. Environmental Research, 30, 1-8.

Ryan, P.H., Dihle, M., Griffin, S., Partridge, C., Hilbert, T.J., Taylor, R., Adjei, S., and Lockey, J.E. (2011) Erionite in road gravel associated with interstitial and pleural changes – An occupational hazard in Western United States. Journal of Occupation and Environmental Medicine, 53, 892-898.

Sabine, T.M., Hunter, B.A., Sabine, W.R., and Ball, C.J. (1998) Analytical expressions for the transmission factor and peak shift in absorbing cylindrical specimens. Journal of Applied Crystallography, 31, 47-51.

Sheppard, R.A. (1996) Occurrences of erionite in sedimentary rocks of the Western United States. U.S. Geological Survey Open-File Report 96-018, 24 pp.

Sherry, H.S. (1979) Ion-exchange properties of the natural zeolite erionite. Clays and Clay Minerals, 27, 231-237.

US EPA, and NDDH (2010) Radiographic changes associated with exposure to erionite in road gravel in North Dakota, Contract EP-R8-06-02/TO#0804, pp. 90.

Yang, H., Bocchetta, M., Kroczynska, B., Elmishad, A.G., Chen, Y., Liu, Z., Bubici, C., Mossman, B.T., Pass, H.I., Testa, J.R., Franzoso, G., and Carbone, M. (2006) TNF-α inhibits asbestos-induced cytotoxicity via a NF- κB-dependent pathway, a possible mechanism for asbestos-induced oncogenesis. Proceedings of the National Academy of Sciences, 103, 10397-10402.

Yang, H., Rivera, Z., Jube, S., Nasu, M., Bertino, P., Goparaju, C., Franzoso, G., Lotze, M.T., Krausz, T., Pass, H.I., Bianchi, M.E., and Carbone, M. (2010) Programmed necrosis induced by asbestos in human mesothelial cells causes high-mobility group box 1 protein release and resultant inflammation. Proceedings of the National Academy of Sciences, 107, 12611-12616.

Young, R.A. (1993) Introduction to the Rietveld method: In: Young RA (ed) The Rietveld method. Oxford University Press, Oxford, pp 1-38.

529 **TABLE 1**. Results of quantitative SEM-EDX microanalyses of erionite from Rome, Oregon.

530

		ALF		Gamble's		
	Start	2 days ALF-48h	4 months ALF-4m	2 days G-48h	15 days G-15d	4 months G-4m
SiO_2	59.43 (57.38-60.71)	59.40 (58.65-60.15)	59.75 (59.20-60.40)	59.25 (58.31-59.71)	59.02 (58.07-60.68)	58.55 (57.88-59.14)
Al_2O_3	13.06 (12.31-14.03)	12.92 (12.42-13.38)	13.07 (12.84-13.37)	13.08 (12.80-13.37)	12.92 (12.38-13.76)	13.69 (13.13-14.22)
CaO	-	-	-	1.37 (1.07-1.66)	-	-
MgO	0.73 (0.57-1.15)	0.59 (0.48-0.66)	0.43 (0.30-0.59)	0.65 (0.55-0.80)	0.46 (0.34-0.63)	0.55 (0.42-0.68)
Na_2O	4.65 (3.59-5.77)	4.80 (4.21-5.31)	4.33 (3.80-5.00)	3.03 (2.24-3.56)	3.83 (2.97-4.92)	4.84 (4.47-5.40)
K_2O	3.63 (3.17-4.29)	3.79 (3.30-4.05)	3.91 (3.71-4.16)	4.12 (3.87-4.51)	5.27 (4.69-6.24)	3.87 (3.36-4.34)
H_2O	18.50	18.50	18.50	18.50	18.50	18.50
total	100.00	100.00	100.00	100.00	100.00	100.00
	Unit-cell content					
Si	28.60 (27.94-29.05)	28.65 (28.37-28.96)	28.55 (28.43-28.63)	28.57 (28.38-28.84)	28.61 (28.17-28.90)	28.22 (27.99-28.53)
Al	7.40 (6.95-8.06)	7.35 (7.04-7.63)	7.45 (7.37-7.57)	7.43 (7.15-7.62)	7.39 (7.10-7.83)	7.78 (7.47-8.01)
Ca	-	-	-	0.71 (0.53-1.03)	-	-
Mg	0.53 (0.41-0.81)	0.42 (0.34-0.48)	0.29 (0.22-0.43)	0.47 (0.31-0.74)	0.33 (0.25-0.45)	0.40 (0.30-0.49)
Na	4.34 (3.32-4.72)	4.49 (3.53-5.01)	4.22 (4.02-4.67)	2.83 (1.51-3.35)	3.60 (2.94-4.66)	4.56 (4.17-5.09)
K	2.23 (1.94-2.62)	2.33 (2.03-2.48)	2.40 (2.26-2.55)	2.53 (2.00-2.80)	3.26 (2.88-3.90)	2.40 (2.05-2.68)
O	72.11 (71.68-72.34)	72.16 (71.74-72.34)	71.88 (71.72-72.25)	72.14 (71.64-72.40)	72.07 (71.76-72.39)	71.96 (71.65-72.21)
H_2O	29.69	29.77	29.65	29.75	29.97	29.74
R	0.794 (0.776-0.807)	0.796 (0.788-0.804)	0.793 (0.790-0.795)	0.794 (0.789-0.798)	0.795 (0.782-0.803)	0.784 (0.777-0.792)
M/(M+D)	0.926 (0.881-0.945)	0.941 (0.929-0.954)	0.958 (0.942-0.968)	0.820 (0.771-0.853)	0.954 (0.932-0.968)	0.946 (0.930-0.958)
Na/M	0.661 (0.559-0.702)	0.653(0.608-0.672)	0.637 (0.612-0.666)	0.528 (0.494-0.583)	0.525 (0.454-0.610)	0.655 (0.634-0.679)
E%	-2.8 (-8.7/9.3)	-4.2 (-8.4/8.0)	3.8 (-6.0/8.0)	-3.7 (-9.9/4.5)	-1.9 (-9.7/6.5)	1.09 (-4.9/9.5)

531

$\Sigma_{cat.}$ s.s. (e^-)	96.4	98.8	95.5	99.1	105.5	100.6
species	-Na	-Na	-Na	-Na	-Na	-Na

532

533

534 **TABLE 2**. Miscellaneous data of the Rietveld refinements. Statistical parameters as defined in
535 Young (1993).

536

	Start	ALF-48h	ALF-4m	G-48h	G-15d	G-4m
2θ range (°)			5-145			
Step size (°2θ)			0.022			
Counting time (s)			30			
R_{Bragg} (%)	0.356	0.324	0.388	0.414	0.443	0.461
R_p (%)	0.976	0.951	1.244	1.228	0.980	1.081
R_{wp} (%)	1.270	1.239	1.634	1.580	1.287	1.416
GoF	1.731	1.456	1.649	1.578	1.650	1.814

537

538

539 **TABLE 3**. Cell parameters and microstructural parameters of erionite-Na before and after leaching.

540

	a (Å)	*c* (Å)	*c/a*	*volume* (Å^3)	L_{vol} (nm)	ε_0
Start	13.23146(10)	15.06142(16)	1.13831(1)	2283.56(4)	473(16)	0.0745(14)
ALF-48h	13.21883(11)	15.08126(14)	1.14089(1)	2282.20(4)	318(8)	0.0752(17)
ALF-4m	13.22000(9)	15.07885(12)	1.14060(1)	2282.24(4)	374(9)	0.0734(13)
G-48h	13.22027(9)	15.07648(12)	1.14041(1)	2281.98(4)	436(13)	0.0713(13)
G-15d	13.22161(12)	15.07014(16)	1.13981(1)	2281.48(5)	337(11)	0.0774(19)
G-4m	13.23126(17)	15.06499(21)	1.13859(1)	2284.03(7)	239(8)	0.0864(22)

541

542

543 **TABLE 4**. Mean <T-O> bond distances, Si/Al distribution, and R value from: 1) SEM EDX
544 microanalyses; 2) Jones' determinative curves (Jones 1968); 3) Alberti's procedure (Alberti et al.
545 1990); 4) regression equation from cell volume data (Passaglia et al. 1998).

546

						R = Si/(Si+Al)			
	<T1-O>	<T2-O>	T1	T2	T1+T2	1	2	3	4
Start	1.630(3)	1.652(4)	$Al_{4.12}Si_{19.88}$	$Al_{3.68}Si_{8.32}$	$Al_{7.80}Si_{28.20}$	0.794(11)	0.783(19)	0.804	0.788
ALF-48h	1.629(4)	1.650(5)	$Al_{3.90}Si_{20.10}$	$Al_{3.59}Si_{8.41}$	$Al_{7.49}Si_{28.51}$	0.796(6)	0.792(22)	0.815	0.790
ALF-4m	1.631(3)	1.644(4)	$Al_{4.19}Si_{19.81}$	$Al_{3.09}Si_{8.91}$	$Al_{7.28}Si_{28.72}$	0.793(2)	0.798(19)	0.818	0.790
G-48h	1.629(3)	1.641(3)	$Al_{3.90}Si_{20.10}$	$Al_{2.87}Si_{9.13}$	$Al_{6.77}Si_{29.23}$	0.794(3)	0.812(19)	0.836	0.791
G-15d	1.630(4)	1.650(5)	$Al_{4.12}Si_{19.88}$	$Al_{3.59}Si_{8.41}$	$Al_{7.71}Si_{28.29}$	0.795(3)	0.786(22)	0.813	0.791
G-4m	1.627(4)	1.656(5)	$Al_{3.59}Si_{20.41}$	$Al_{4.03}Si_{7.97}$	$Al_{7.62}Si_{28.38}$	0.784(3)	0.788(22)	0.810	0.787
average	*1.629(1)*	*1.649(6)*	$Al_{3.97}Si_{20.03}$	$Al_{3.48}Si_{8.52}$	$Al_{7.45}Si_{28.55}$	*0.793(4)*	*0.793(10)*	*0.816(10)*	-

547

548

549 **TABLE 5**. T-O-T bond angles (°).

550

T-O-T (°)	Start	ALF-48h	ALF-4m	G-48h	G-15d	G-4m	*average*
Si1-O1-Si2	141.8(3)	142.0(4)	142.2(3)	143.2(3)	143.1(4)	141.6(4)	*142.3(6)*
Si1-O2-Si1	139.6(4)	139.9(5)	141.0(3)	140.4(3)	137.7(5)	139.5(5)	*139.7(10)*
Si1-O3-Si1	141.9(4)	142.7(5)	142.2(4)	144.1(3)	142.5(5)	144.8(6)	*143.0(10)*
Si1-O4-Si1	148.9(3)	148.6(4)	149.6(3)	149.0(3)	148.4(4)	148.8(4)	*148.9(4)*
Si2-O5-Si2	145.7(5)	145.7(7)	146.8(5)	148.2(5)	147.0(7)	142.2(7)	*145.9(19)*
Si2-O6-Si2	171.0(5)	170.3(6)	170.4(5)	169.5(5)	169.6(7)	172.6(7)	*170.6(10)*

551

552

553 **TABLE 6**. Refined site scattering *s.s.* (e^-) for both EF cation and water molecule sites.

554

s.s.	Start	ALF-48h	ALF-4m	G-48h	G-15d	G-4m
Ca1 (e^-)	30.9(6)	5.1(17)	5.4(12)	10.5(10)	13.3(18)	28.5(10)
Ca2 (e^-)	30.1(5)	35.7(7)	33.0(6)	29.2(8)	33.5(6)	30.4(6)
Ca3 (e^-)	-	-	-	11.4(11)	-	-
K2 (e^-)	15.8(9)	12.9(9)	15.4(9)	13.5(9)	19.4(12)	19.7(11)
Σ_{cat} (e^-)	114.8(20)	92(3)	92(3)	103(4)	104(3)	117(3)
OW7 (e^-)	19(3)	37.4(17)	36.6(15)	41.1(16)	41.5(16)	21.3(37)
OW8 (e^-)	47.5(7)	32.4(13)	31.0(9)	34.7(11)	39.2(9)	47.8(9)
OW9 (e^-)	50(3)	51(5)	38.4(25)	30(3)	34(4)	52.7(29)
OW10 (e^-)	36(3)	56(3)	54(3)	69(3)	54(4)	30.0(35)
OW11 (e^-)	53(3)	46.5(19)	41.5(16)	29.9(19)	41.7(19)	50.5(36)
OW12 (e^-)	54.1(21)	54(6)	69.6(24)	66.6(24)	64(3)	56.2(31)
Σ_{water} (e^-)/*apfu*	259(17)/*32.4(21)*	277(19)/*34.6(24)*	271(12)/*33.8(15)*	272(13)/*34.0(16)*	275(15)/*34.4(19)*	259(18)/*32.4(21)*

555

556

557 **TABLE 7**. Proposed site partition from combined SEM-EDX data (1) and structure refinements (2).

558 Ions population expressed as Ca, Mg, Na, and K *apfu*. Site scattering (*s.s.*) in e^-.

559

Sample	Sites	Ca	Mg	Na	K	1 (*s.s.*)	2 (*s.s.*)
Start	Ca1	-	0.53	1.60	-	24.0	30.9(6)
	Ca2	-	-	2.74	-	30.1	30.1(5)
	Ca3	-	-	-	-	-	-
	K1	-	-	-	2.00	38.0	38.0
	K2	-	-	-	0.23	4.4	15.8(9)
	Σ_{cat}					96.5	115(2)
	H_2O						259(17)
ALF-48h	Ca1	-	0.42		-	5.0	5.1(17)
	Ca2	-	-	3.25	-	35.7	35.7(7)
	Ca3	-	-	-	-	-	-
	K1	-	-	-	2.00	38.0	38.0
	K2	-	-	-	0.33	6.3	12.9(9)
	diffuse			1.24		13.6	
	Σ_{cat}					98.7	92(3)
	H_2O						277(19)
ALF-4m	Ca1	-	0.29		-	3.5	5.4(12)
	Ca2	-	-	3.00	-	33.0	33.0(6)
	Ca3	-	-	-	-	-	-
	K1	-	-	-	2.00	38.0	38.0
	K2	-	-	-	0.40	7.6	15.4(9)
	diffuse			1.22		13.4	
	Σ_{cat}					95.5	92(3)
	H_2O						271(12)
G-48h	Ca1	-	0.47	0.18	-	7.6	10.5(10)
	Ca2	-	-	2.65	-	29.2	29.2(8)
	Ca3	0.71	-	-	-	14.2	11.4(11)

	K1	-	-	-	2.00	38.0	38.0
	K2	-	-	-	0.53	10.1	13.5(9)
	Σ_{cat}					99.1	103(4)
	H_2O						272(13)
G-15d	Ca1	-	0.33	0.55	-	10.0	13.3(18)
	Ca2	-	-	3.05	-	33.6	33.5(6)
	Ca3	-	-	-	-	-	-
	K1	-	-	-	2.00	38.0	38.0
	K2	-	-	-	1.26	23.9	19.4(12)
	Σ_{cat}					105.5	104(3)
	H_2O						275(15)
G-4m	Ca1	-	0.40	1.80	-	24.6	28.5(10)
	Ca2	-	-	2.76	-	30.4	30.4(6)
	Ca3	-	-	-	-	-	-
	K1	-	-	-	2.00	38.0	38.0
	K2	-	-	-	0.40	7.6	19.7(11)
	Σ_{cat}					100.6	117(2)
	H_2O						259(18)

560

561

562

Figure captions

FIGURE 1. (**a**) Diffraction patterns collected on material recovered after different settling times. Relevant reflections of impurities are labeled as follow: Cl: clay minerals; Q: quartz; F: feldspars; (**b**) Dependence of the intensity of the iron fluorescence lines from settling time, as collected at the multichannel analyzer of the solid-state detector. Data were rescaled on the basis of the common CuKα fluorescence line. The absence of the CuKβ fluorescence line is due to its removal by the incident beam multilayer (Göbel) mirrors.

FIGURE 2. Rietveld plots of (**a**) starting erionite-Na; erionite after leaching for 4 months with ALF (**b**) and Gamble's solution (**c**).

FIGURE 3. SEM image of erionite-Na fibers. Inbox: magnified view showing the fibrils constituting the fiber.

FIGURE 4. Location of the EF cation sites within the erionite framework. Water molecules sites removed for clarity.

FIGURE 5. Ortep-3 (Farrugia 1997) plot illustrating the coordination of Ca1, Ca2, and K2 sites in erionite-Na. On the left side: possible mutual distribution of EF cations and oxygen atoms, pertaining to both framework or water molecules, occurring in the case of Na located at Ca1. This pattern is compatible with the occurrence of K2. On the right side: presence of Mg at Ca1 is incompatible with the occurrence of both K2 and Ca2 due to short K2-OW9 and OW8-OW9 contacts, respectively.

FIGURE 6. Schematic representation of the various cations motion/exchange processes occurring during leaching of erionite-Na with ALF and Gamble's solutions; **(a)** START: untreated erionite-Na; (**b**) ALF-48h and (**c**) ALF-4m: segregation of all available Mg^{2+} at Ca1 site and corresponding migration of Na^{+} from Ca1 to Ca2 and towards alternative sites located near water molecule sites (dotted ellipse); (**d**) G-48h: $Ca^{2+} \rightarrow Na^{+}$ exchange occurring *via* release of Na^{+} from Ca1 and fixing of Ca^{2+} at Ca3; (**e**) G-15d: $Na^{+} \rightarrow Ca^{2+}$ exchange occurring *via* removal of Ca^{2+} from Ca3 and fixing of Na^{+} at both Ca1 and Ca2; (**f**) G-4m: restoring of the starting EF cations population with

589 migration of Na^+ from Ca2 to Ca1. Minor difference represented by an increase of the K^+ content at
590 K2 site (not shown) located at the center of the boat-shaped 8MR.

591 **FIGURE 7**. Comparison of the diffraction patterns of the starting material and of the Gamble's
592 leached samples. Patterns are vertically displaced for clarity. Grey areas located at approximately 8-
593 9 °2θ are caused by the presence of amorphized erionite. The relevant reflection of calcite at ca.
594 29.5 °2θ, precipitated from the solution, is arrowed.

595

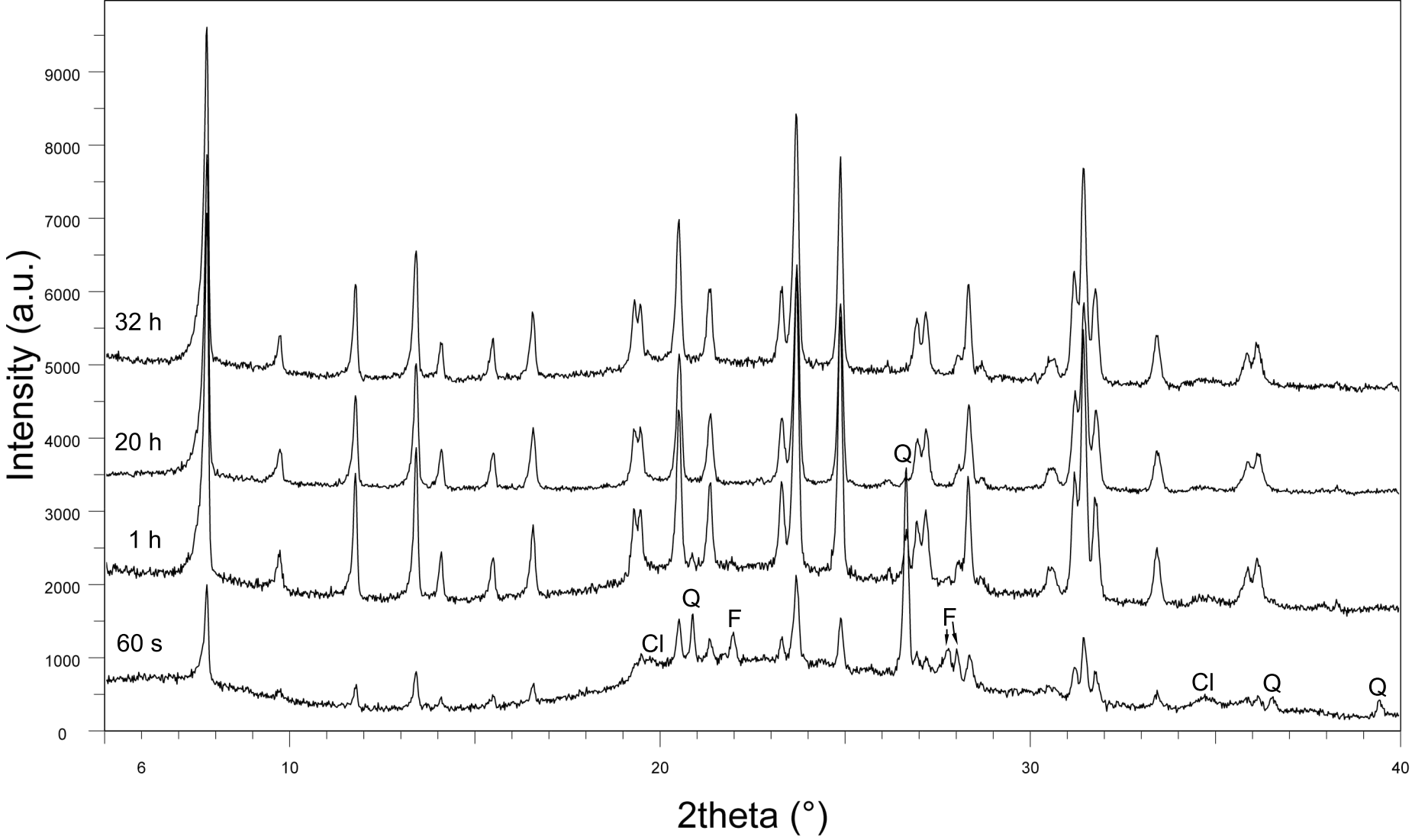
Intensity (a.u.)
9000
8000
7000
6000
5000
4000
3000
2000
1000
0
32 h
20 h
1 h
60 s
Q
Cl
Q
F
F
Cl
Q
Q
6
10
20
30
40
2theta (°)

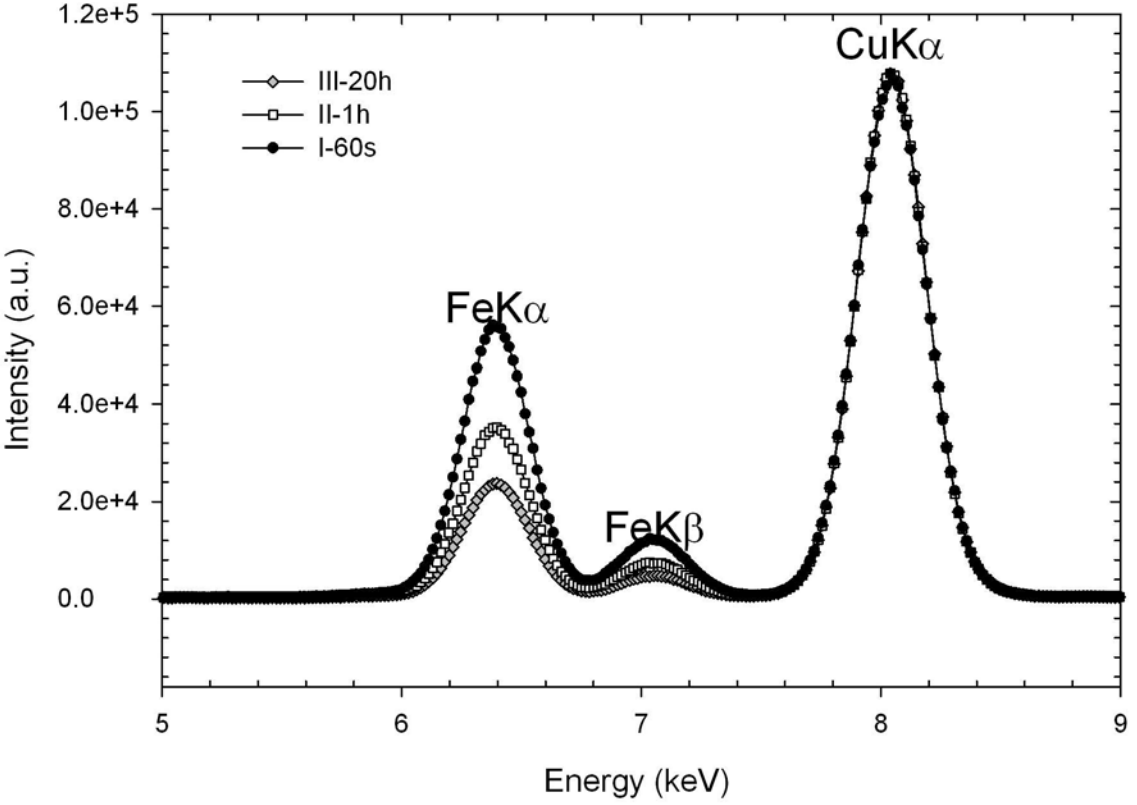
1.2e+5
1.0e+5
8.0e+4
6.0e+4
4.0e+4
2.0e+4
0.0
Intensity (a.u.)
III-20h
II-1h
I-60s
FeKα
FeKβ
CuKα
5
6
7
8
9
Energy (keV)

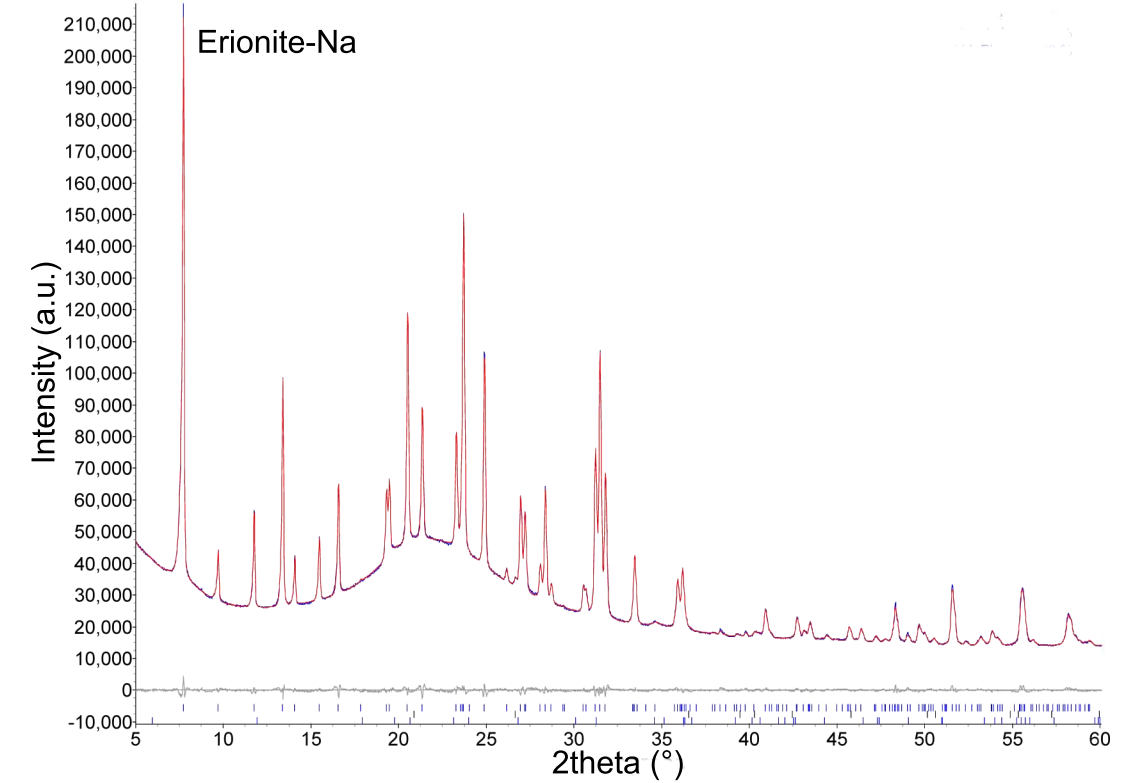
Erionite-Na
Intensity (a.u.)
210,000
200,000
190,000
180,000
170,000
160,000
150,000
140,000
130,000
120,000
110,000
100,000
90,000
80,000
70,000
60,000
50,000
40,000
30,000
20,000
10,000
0
-10,000
5
10
15
20
25
30
35
40
45
50
55
60
2theta (°)

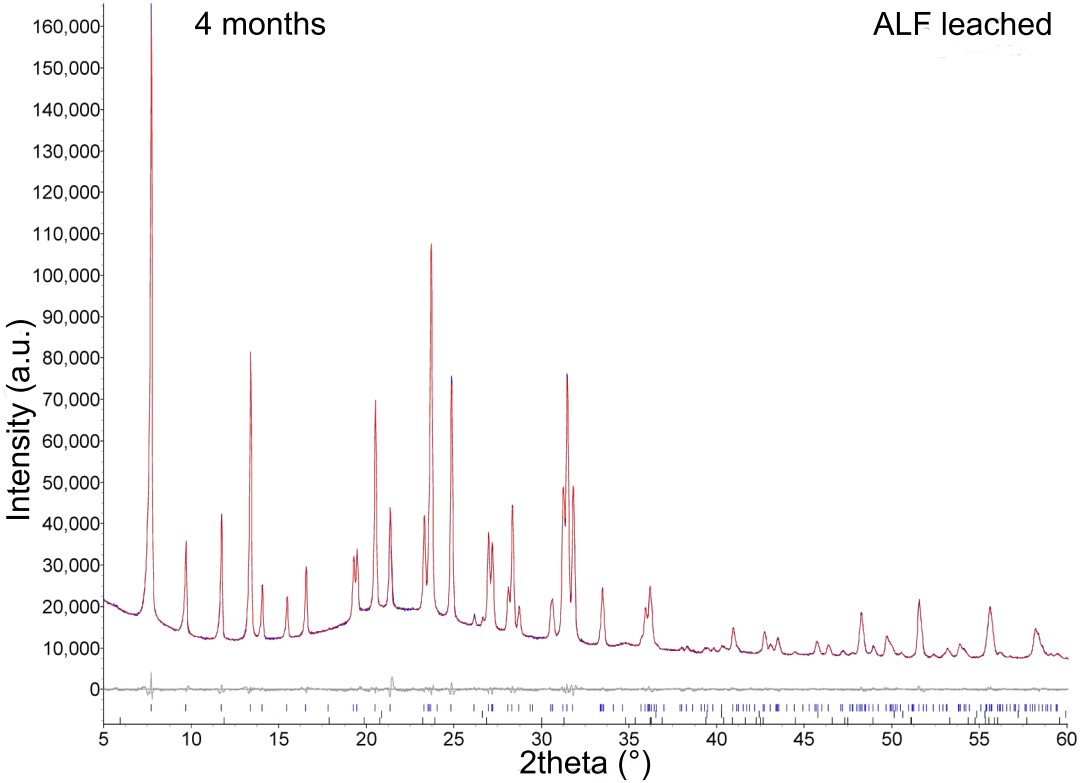
4 months
ALF leached
Intensity (a.u.)
160,000
150,000
140,000
130,000
120,000
110,000
100,000
90,000
80,000
70,000
60,000
50,000
40,000
30,000
20,000
10,000
0
5
10
15
20
25
30
35
40
45
50
55
60
2theta (°)

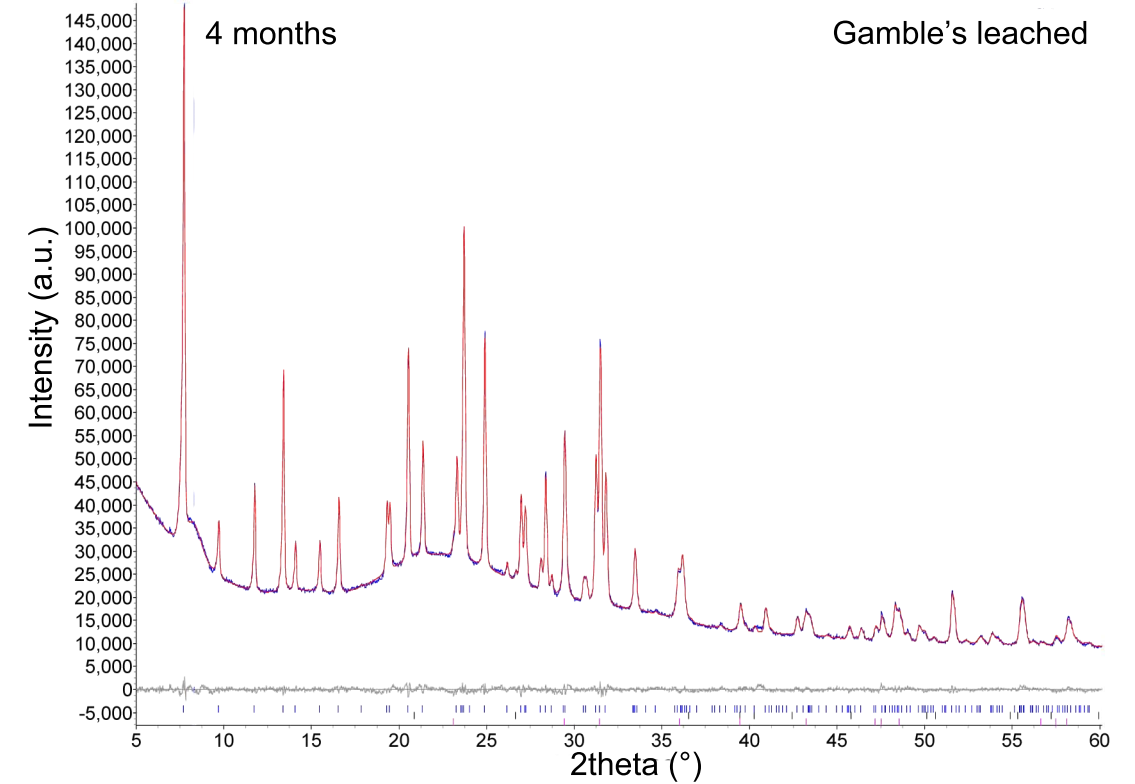
4 months
Gamble's leached
Intensity (a.u.)
145,000
140,000
135,000
130,000
125,000
120,000
115,000
110,000
105,000
100,000
95,000
90,000
85,000
80,000
75,000
70,000
65,000
60,000
55,000
50,000
45,000
40,000
35,000
30,000
25,000
20,000
15,000
10,000
5,000
0
-5,000
5
10
15
20
25
30
35
40
45
50
55
60
2theta (°)

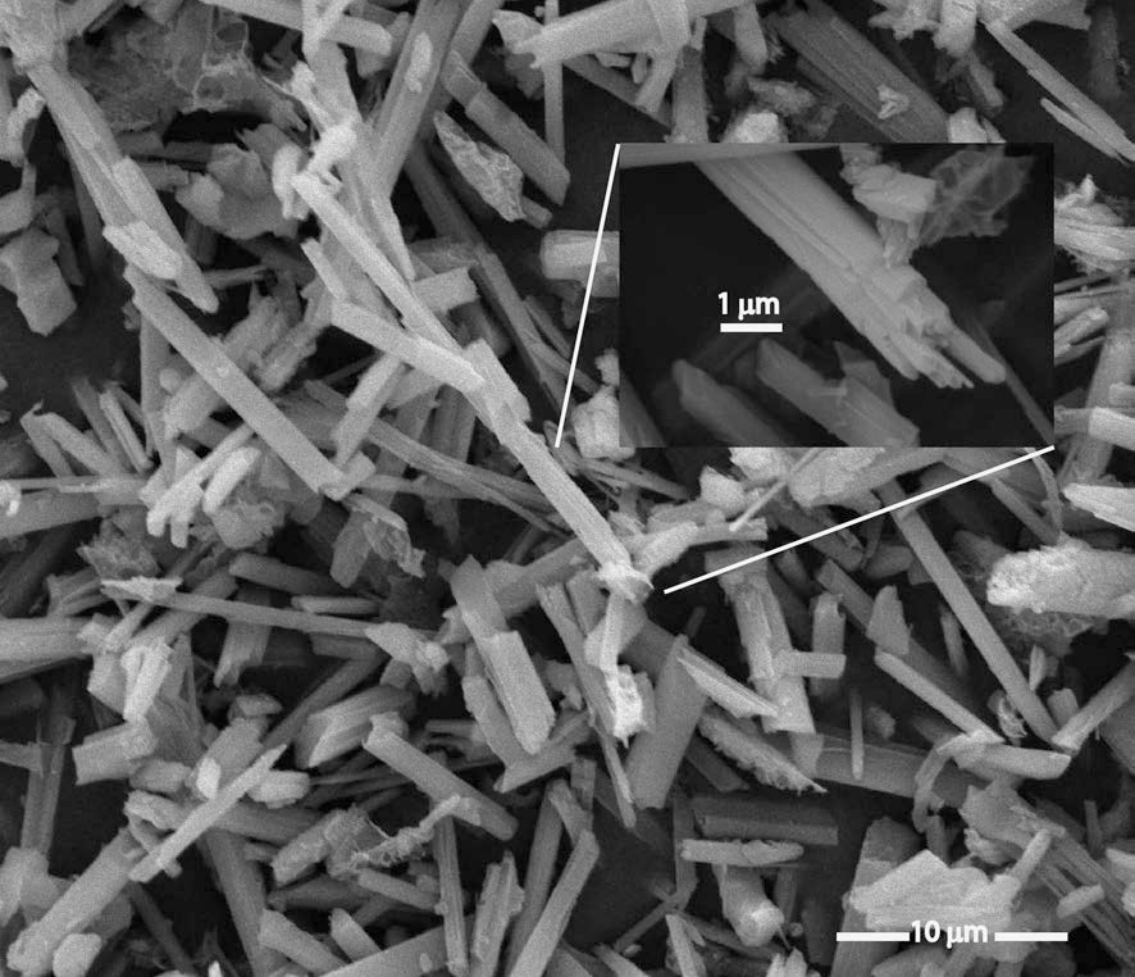
1 µm
10 µm

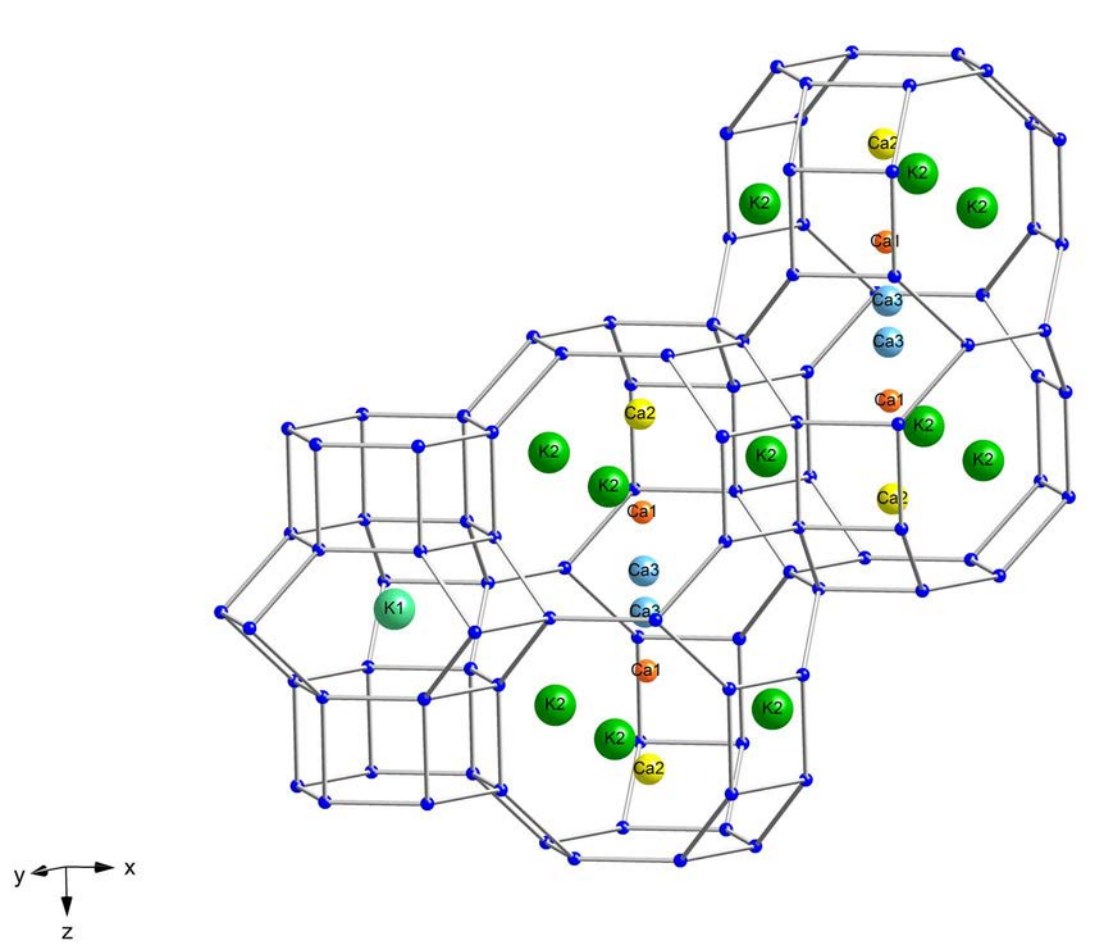
Ca2
K2
K2
K2
Ca1
Ca3
Ca3
Ca1
K2
K2
K2
K2
Ca2
Ca2
K2
Ca1
Ca3
K1
Ca3
Ca1
K2
K2
K2
Ca2
y
x
z

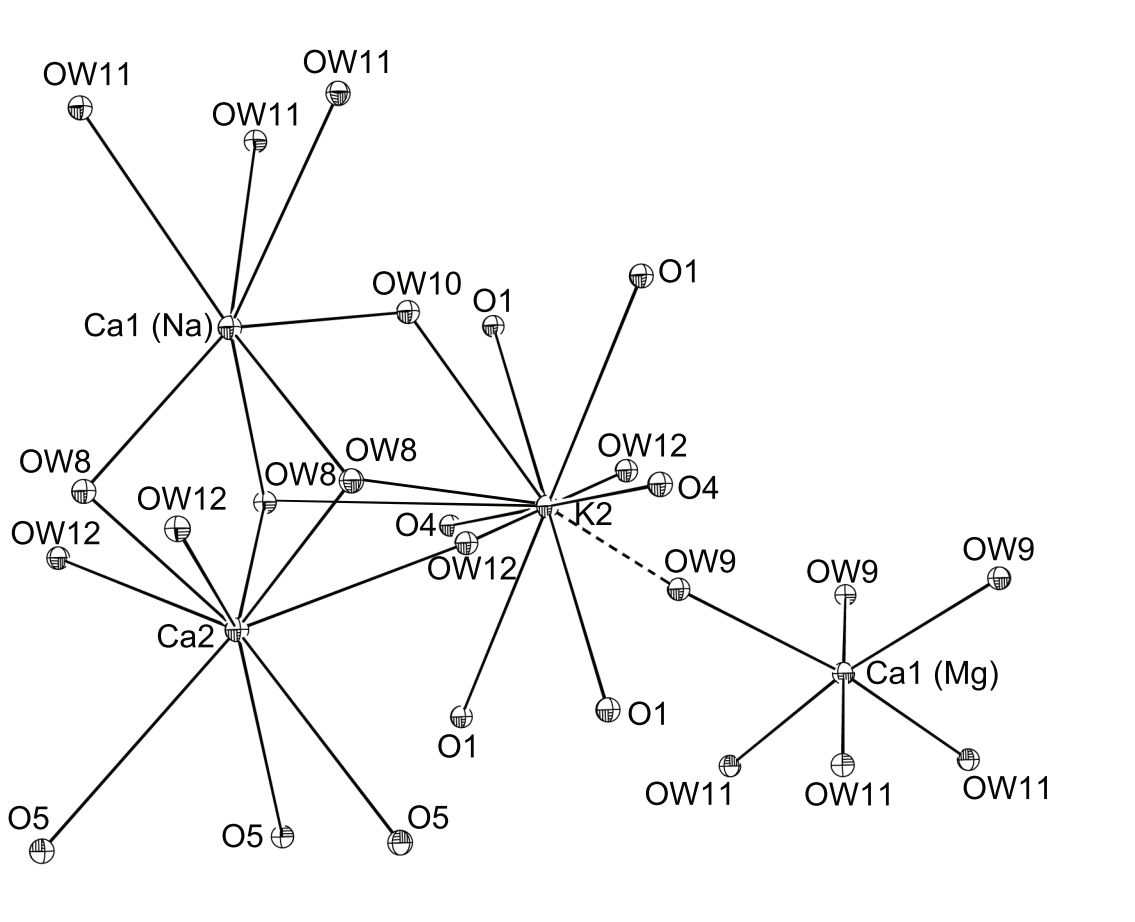
OW11
OW11
OW11
Ca1 (Na)
OW10
O1
O1
OW8
OW8
OW8
OW12
O4
OW12
OW12
O4
K2
OW12
OW9
OW9
OW9
Ca2
Ca1 (Mg)
O1
O1
OW11
OW11
OW11
O5
O5
O5

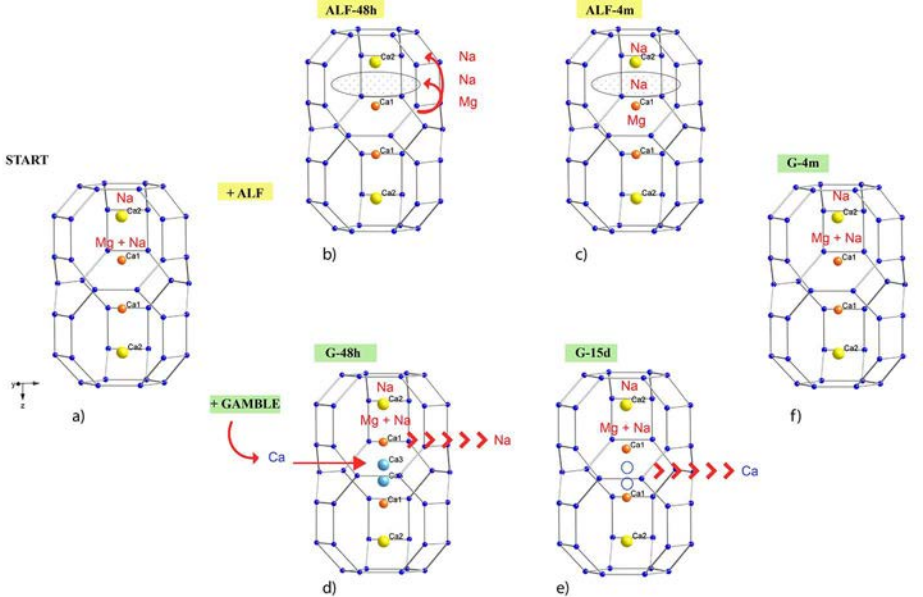
START
Na
Mg + Na
Ca1
Ca2
a)
+ ALF
ALF-48h
Na
Na
Mg
b)
ALF-4m
Na
Na
Mg
c)
G-4m
Na
Mg + Na
f)
+ GAMBLE
Ca
G-48h
Na
Mg + Na
Ca3
d)
G-15d
Ca
e)

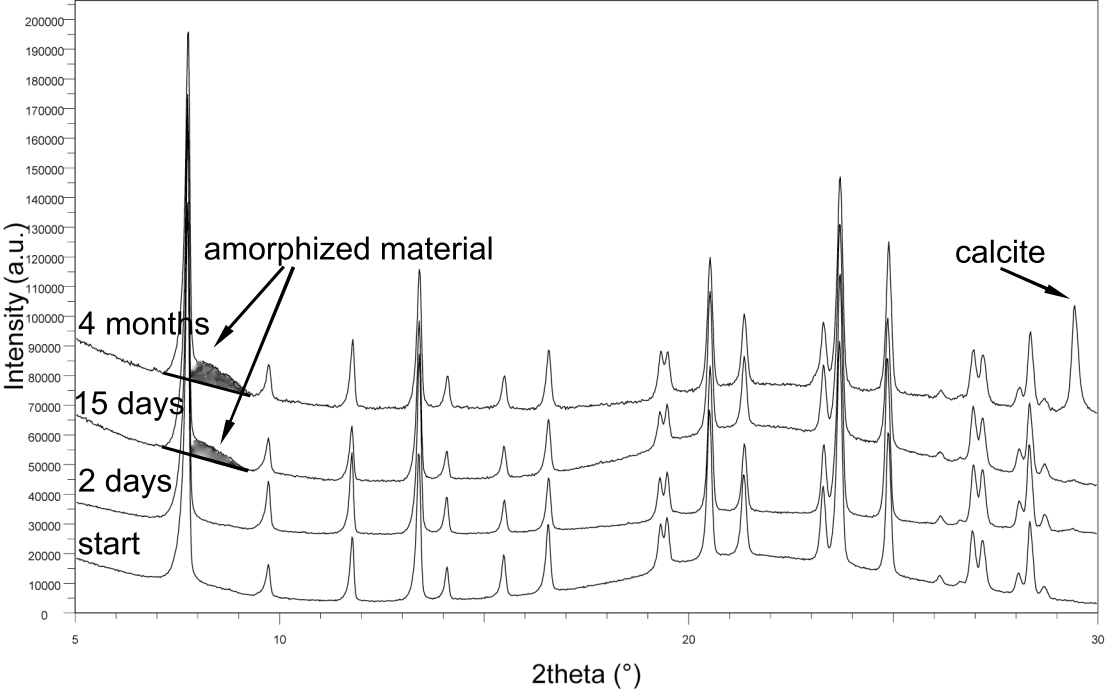
Intensity (a.u.)
2theta (°)
amorphized material
calcite
4 months
15 days
2 days
start